Characterization of Nanometer-Sized Oxygen Precipitates in Highly B-Doped Czochralski Silicon

Dawid Kot,* Gudrun Kissinger, Markus Andreas Schubert, Steffen Marschmeyer, Georg Schwalb, and Andreas Sattler

We use a wide variety of analytical methods to characterize nanometer-sized oxygen precipitates in highly B-doped Czochralski (CZ) silicon. Due to the enhanced precipitation of oxygen in this type of wafer, the precipitate density reaches a value of $1 \times 10^{13}\,\mathrm{cm}^{-3}$ already after short annealing. On the one hand, this provides an excellent possibility for testing the detection limits of different methods and on the other hand the knowledge on oxygen precipitation in p^+ material can be broadened. In order to study density, size, and morphology of oxygen precipitates, we exploit scanning transmission microscopy (STEM), reactive ion etching (RIE), and preferential etching. STEM is also used to determine size distribution and energy dispersive X-ray spectroscopy (EDX) and electron energy loss spectroscopy (EELS) are used to investigate the composition of oxygen precipitates. In annealed samples, oxygen precipitates, dislocation loops, and stacking faults are found. The dislocation loops disappear after long annealing in contrast to the stacking faults which are detected in all samples annealed at 1000 °C. It is found that the long anneal at 1000 °C leads to the formation of two size fractions of precipitates. This process is similar to Ostwald ripening. The precipitates are octahedral, consist of SiO_2 and the B concentration is below the detection limit of the methods used here. The obtained results are in good agreement with the nucleation model of highly doped wafers proposed by Sueoka.

1. Introduction

Epitaxial wafers are used for exceptional application in order to enhance the devices yield.[1] The epi layers are often deposited on heavily boron doped wafers (p^+). This kind of substrate possesses high getter efficiency for metallic impurities and an enhanced nucleation of oxygen precipitates which can also contribute to gettering.[2–5] Because of the very high density of precipitate nuclei, it can easily happen that the interstitial oxygen is consumed before the oxide precipitates exceed the detection limit of common analysis techniques like preferential etching.

The high doping level of the substrate is also a problem for delineation of defects for some etchants like e.g., Secco etchant[6] which usually is a very good etchant for the moderately doped substrate (p^-) but it causes a rugged surface if used on the heavily boron doped wafer. Moreover, a high concentration of free carriers is limiting the Fourier transform infrared (FTIR) spectroscopy, especially for the measurement of the concentration of interstitial oxygen. It is also impossible to study the morphology of oxygen precipitates by FTIR which is easily possible in moderately doped wafers.[7,8] In order to overcome the problems appearing during investigation of highly doped wafers one uses advanced investigation methods and etching solutions.

The application of many analytical methods is important for understanding some open issues like the nucleation mechanism in highly boron doped silicon. In the literature, a variety of models explaining the enhanced nucleation in p^+ substrates were proposed. In Ref. [9], the nucleation is explained via the reaction $2Si + 2O_i \leftrightarrow SiO_2 + I_{Si}$. This reaction is driven to the right side due to lower formation energy of Si self-interstitials in p^+ silicon. Wijaranakula[10] proposed a mechanism where B_iO_i pairs are assumed as a mobile species which dissociates in the vicinity of the precipitate relaxing and reducing the strain and the surface energy. In another approach, proposed by Takeno et al.,[4] B incorporated in the precipitate reduces the strain which is due to the different volume between precipitate and silicon matrix. Accordingly, the reaction can be written as follows $(1 + \alpha)Si + 2Oi + \beta V + \gamma B \leftrightarrow SiO_2B_\gamma + \alpha I$ where γ is the fraction of B atoms absorbed to the precipitate. This was observed by De Gryse et al.[11] who found by FTIR analysis that the precipitates in highly B-doped silicon consist with high probability of a mixture of SiO_2 and B_2O_3 with a high volume fraction of B_2O_3. For B-doped material with $8\,\mathrm{m\,\Omega\,cm}$, they determined a volume fraction of 40% B_2O_3.[12] In order to answer at least partially the question about the nucleation mechanism in p^+ material, the knowledge about the composition of oxygen precipitates is essential.

The enhanced nucleation in p^+ wafer raises another question regarding the growth behavior of whether Oswald ripening

Dr. D. Kot, Dr. G. Kissinger, Dr. M. A. Schubert, Dr. S. Marschmeyer
IHP
Im Technologiepark 25, 15236 Frankfurt (Oder), Germany
E-mail: kot@ihp-mictoelectronics.com

Dr. G. Schwalb, Dr. A. Sattler
Siltronic AG
Hanns-Seidel-Platz 4, 81737 München, Germany

**ADVANCED
SCIENCE NEWS**

www.advancedsciencenews.com

pss
physica status solidi c

www.pss-c.com

occurs if the wafer is annealed long enough.[13] In X-ray Pendellösung fringes measurement of the silicon crystals, for the annealing time up to 100 h at 900 °C, the authors interpreted their results in terms of Ostwald ripening.[14] In order to shed some light on this issue, we also studied the precipitate size distribution.

In this work, we applied different analytical techniques like scanning transmission electron microscopy (STEM), reactive ion etching (RIE) and cleave and etch techniques to characterize the nanometer-sized oxygen precipitates and to solve a few questions mentioned above. The samples used in the experiment were first annealed at 780 °C for 3 h to stabilize the precipitate nuclei and then these nuclei were grown at 1000 °C during isothermal annealing. The size distribution, morphology, and density of the oxide precipitates were determined by STEM. The composition of the precipitates was investigated by energy dispersive X-ray spectroscopy (EDX) and electron energy loss spectroscopy (EELS). Moreover, reactive ion etching (RIE) and cleave and etch (C&E) techniques were used to detect oxide precipitates. Here, preferential etchants with a different sensitivity were compared. RIE is suitable for detection of oxide precipitates because of their masking effect based on the available high oxide to silicon selectivity.[15] Moreover, the EDX and EELS studies helped to find out if considerable amounts of boron are incorporated into the oxide precipitates for strain relaxation.

2. Experimental Section

2.1. Samples

B-doped (100) Czochralski-Si wafers with resistivity of about 8.5 mΩ cm, and an initial O_i concentration of 5.3×10^{17} cm^{-3} (determined by gas fusion analysis, were used for the experiments). The wafers were annealed at 780 °C for 3 h to stabilize precipitate nuclei and then these nuclei were grown at 1000 °C for 0, 0.5, 1, 2, 16, 32, and 64 h in N_2.

2.2. RIE

The etch experiments were performed with a commercial deep silicon etch system Tegal 200. The gas mixture used was SF_6/C_4F_8. SF_6 is an etching gas which etches silicon isotropic. Therefore, C_4F_8 was added to avoid the isotropic attack of F radicals coming from SF_6 by generation of a sidewall passivation. Such the process is highly anisotropic. The Si/SiO_2 selectivity is ≈25:1. The etched depth was 4.0 μm. After the RIE process, the wafers were ashed and rinsed in Piranha/HF/SC1 solutions to remove the polymers deposited at the cone sidewalls. The density of the pillar-shaped Si cones was investigated by scanning electron microscopy (SEM).

2.3. STEM

A 200 kV STEM FEI Tecnai Osiris equipped with tools EDX analysis and EELS was used to analyze the morphology, density, and size distribution of oxygen precipitates. EEL spectra of the

plasmon losses were taken in the STEM mode using a Gatan Enfina FS-1 spectrometer in order to determine the composition of precipitates. The TEM lamellas thickness was measured by the EELS log-ratio technique[16] which is integrated in the software "DigitalMicrograph" from Gatan.

2.4. C&E

In order to be able to delineate small defects related to oxygen precipitates (20 nm diameter or less) the Cr-free etchants characterized by high selectivity and low etching rate should be apply. In this work, we used two etchants, the Cr-free Toshiba etchant composed of HF (50%): acetic acid (100%): nitric acid (70%) = 1: 12: 4 + 2 g $AgNO_3$ + 4 g $CuNO_3$ + 198 g H_2O[17] and the organic peracid etchant (OPE:C) H_2O_2 (50%): HF (50%): acetic acid (100%) = 1: 1: 2.[18,19]

3. Results and Discussion

3.1. Morphology, Size, and Density

In order to determine bulk micro defect (BMD) density three different methods were used. BMD is a commonly used term for oxygen precipitates with and without secondary defects generated during precipitate growth.

The defects found by STEM investigation are mainly octahedral oxygen precipitates. Small octahedral precipitates are observed in the sample which received only stabilization step at 780 °C for 3 h. Only very few dislocation loops were found in this sample. The dislocation loops appear more frequently already after 0.5 h of growth where they accompany the octahedral precipitates as it is shown in **Figure 1**(a). Because of the fast nucleation, a high amount of Si self-interstitials is ejected from the precipitates. These Si self-interstitials form stacking faults (SF) as demonstrated in Figure 1(b). The formation of SFs is also very fast and it takes place already after 0.5 h of growth at 1000 °C. The dislocation loops disappear for long anneals where only octahedral precipitates and stacking faults remain. Figure 1 shows an example of large octahedral precipitates (c) and stacking faults with large oxygen precipitates (d) in the wafer annealed for 16 h. The same is observed for longer duration of growth steps, for 32 and 64 h.

Besides of morphological information the STEM investigation provides valuable information about the size distribution of the precipitates as shown in **Figure 2**. The size for most of oxygen precipitates is nearly the same in the sample subjected to the stabilization step only. However, the increasing annealing time at 1000 °C broadens the size distribution until it spreads in fractions of large and small precipitates. This was observed in the sample annealed at 1000 °C for 16 h. Further, the fraction split proceeds very slowly but the fraction of very small precipitates is continuously increasing as can be observed in the sample annealed at 1000 °C for 64 h. These results do not give a direct answer of whether the Ostwald ripening occurs or not. If so, it seems to take a very long time since the fraction of the large precipitates grows very slowly.
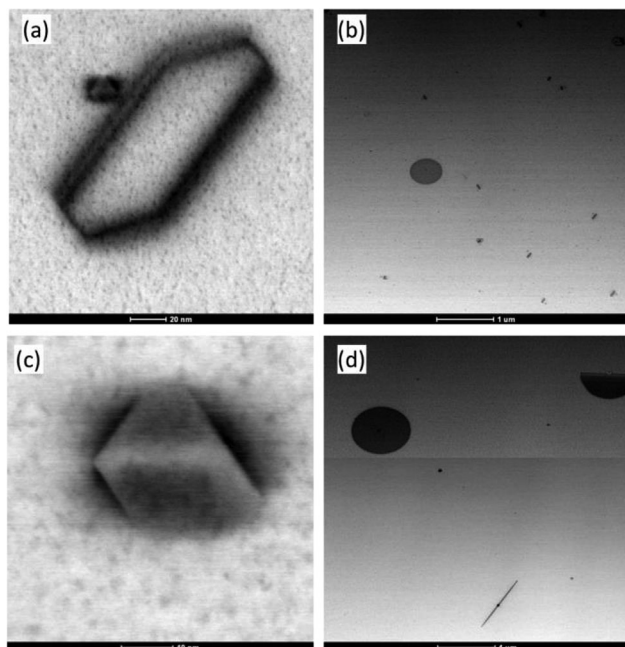
Figure 1. Typical defects observed in the investigated samples. Octahedral oxygen precipitate accompanied by dislocation loop (a), stacking fault and dislocation loops (b), both in samples annealed at 1000 °C for 1 h. Octahedral oxygen precipitates (c), stacking fault and large oxygen precipitates (d) both in samples annealed at 1000 °C for 16 h.

Next, we compared the calculated and the measured size of oxygen precipitates.

In order to calculate the size of oxygen precipitates we used the diffusion limited growth model.[20,21] For the case of oxygen consumption the equation becomes

$$\frac{dr}{dt} = \frac{D_{Oi}}{r}\left[\frac{C_{Oi}(t) - C_{Oi}^{eq}}{C_P}\right] \qquad (1)$$
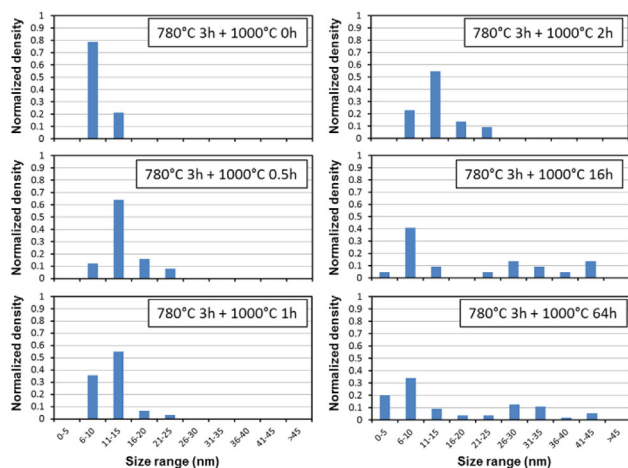
where D_{Oi} is the diffusivity of interstitial oxygen, r is the radius of the oxygen precipitates, $C_{Oi}(t)$ is the time t dependent concentration of interstitial oxygen, C_{Oi}^{eq} is the solubility of interstitial oxygen. C_p is the concentration of oxygen in the precipitates. For D_{Oi} and $C_{Oi}(eq)$ we used data from Ref. [22]. For C_p we used data from Ref. [21]. **Figure 3** shows side length of the octahedral precipitates measured by STEM. Red triangles represent the average size while the blue circles are attributed to the largest observed precipitate. The solid curves represent the calculated values according to Eq. (1) for different concentrations of BMDs. Since the measured precipitate density is about $1 \times 10^{13}\,\mathrm{cm^{-3}}$, there is a good agreement between the measured and calculated values.

Although, STEM investigations provide excellent results the preparation of the samples is very time consuming. The determination of the defect density by this method is practical only if the defect density is sufficiently high or if the size of defects is large enough for a low magnification scanning. For that reason, it is important to develop techniques being an alternative for the STEM investigation. Here, RIE can be a solution. The advantage of this technique is the area of investigation which can be as large as a whole wafer. It is also "clean" compared to the preferential etching technique. The potential of chemical handling hazards is lower than for preferential etching.

The RIE used in this work revealed characteristic pillar-shaped Si cones as can be seen in **Figure 4**. The shape of the cones is caused by the highly anisotropic RIE process. The density of the cones increases with increasing annealing time. However, the density of the cones is over two orders of magnitude lower than that determined by STEM. This is a consequence of the parameters used in the etching process which can still be optimized to enhance the selectivity.

Finally, we used the C&E technique, which is a fast and low cost method. In order to avoid the presence of Cr based oxidizing agents being harmful to health we applied two Cr-free etchants. The Toshiba etchant and OPE:C etchant characterized by fast ($1.63\,\mu\mathrm{m\,min^{-1}}$) and slow ($0.25\,\mathrm{nm\,min^{-1}}$) etching rate, respectively. The etch pits observed under an optical microscope are shown in **Figure 5**. The etch pits in Toshiba etchant are clear and large. The etch pits after etching in OPE:C etchant are smaller

Figure 2. Normalized size distributions of oxygen precipitates determined by STEM.
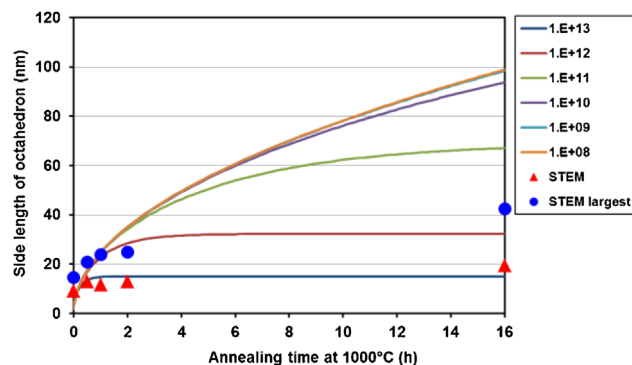
Figure 3. Side length of octahedral precipitates measured by STEM (symbol) and calculated (solid lines).
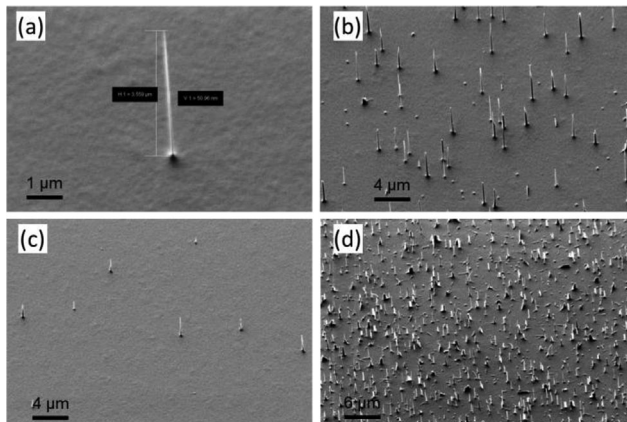
Figure 4. RIE etched surface observed by SEM in samples with anneal steps: 780 °C 3 h + 1000 °C 1 h (a and c), 780 °C 3 h + 1000 °C 2 h (b), 780 °C 3 h + 1000 °C 16 h (d).

due to the etched depth which is about one order of magnitude lower than in the Toshiba etched sample.
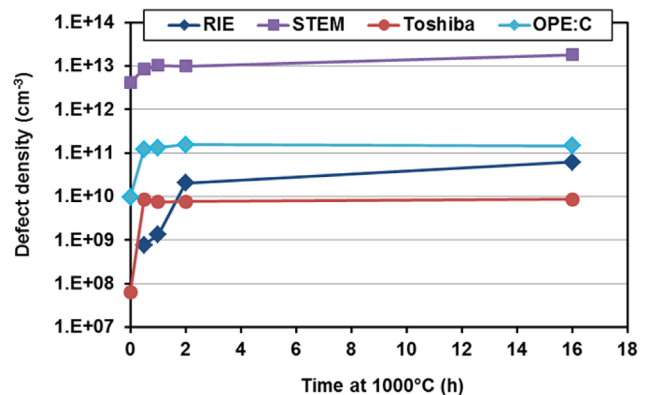
Figure 6 shows comparison of the BMD density determined by all the applied methods in highly boron-doped silicon wafers annealed for different time. The highest density is measured by STEM and it reaches value of 1×10^{13} cm^{-3}. The BMD density remains almost unchanged with the time of the growth anneal at 1000 °C. The BMD density of all the other methods used are far below the STEM values. The best results are indicated by OPE:C etching where the trend of BMD density curve is similar to STEM. The RIE technique used in this work is sensitive to the precipitate size. It reaches a plateau after 2 h of growth. This corresponds to the rise of the maximal size of precipitates in Figure 3 where the size is still increasing. The weakest results are represented by the Toshiba etchant but in this case there is good agreement with the trend of the BMD density curve of STEM.

3.2. Composition of Oxygen Precipitates

Because of the very low fraction of large precipitates, it was impossible to find a precipitate which would meet the conditions required for the investigation of the composition of oxygen precipitates by EDX from Ref. [23] in a thin region of the TEM lamella. The optimum configuration would be that the
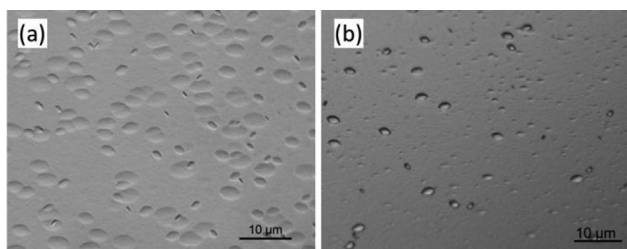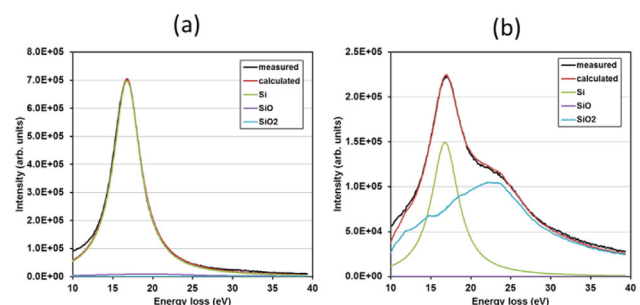

Figure 6. Comparison of BMD density measured by different methods.

precipitate completely passes through the thickness of the investigated sample. This is, however, not the case for the EELS plasmon method.[8] In this method, the composition of the precipitates is determined from the deconvolution of the low loss EEL spectra into reference spectra of Si, SiO, and SiO$_2$. For more detailed information, the reader is referred to Ref. [24].

Figure 7 shows deconvolution of EEL spectra recorded in the center of an octahedral precipitate and in the Si matrix outside of the precipitate. Outside of the precipitate the TEM lamella consist of Si in 97 and 3% of SiO. The SiO content is the result of the native oxide on the TEM lamella. The material in the precipitate is composed of Si 34% and SiO$_2$ 66%. The presence of Si here means that the precipitate does not completely penetrate through the thickness of the investigated sample. SiO was not found in the precipitate.

In order to determine the boron concentration the same octahedral precipitate was measured by EDX. The bright Field image, EDX maps of O and B elements and the EDX spectra measured at two different locations in the oxygen precipitate are shown in **Figure 8**. There is no difference between the spectra in the energy position where the B peak should be located. There is, however, a peak ratio change between Si and O due to the octahedral form of the precipitate. This means that the B concentration is below the detection limit which can be estimated to 10%. This disagrees with results of DeGryse et al.[12] where B in the precipitate was found up to 40% by FTIR.

Figure 5. Etch pits observed after etching for 3 min in Toshiba etchant (a) and after etching for 18 h in OPE:C etchant (b).

Figure 7. Deconvolution of EEL spectra in the Si matrix outside of a precipitate (a), and in the center of a precipitate (b).
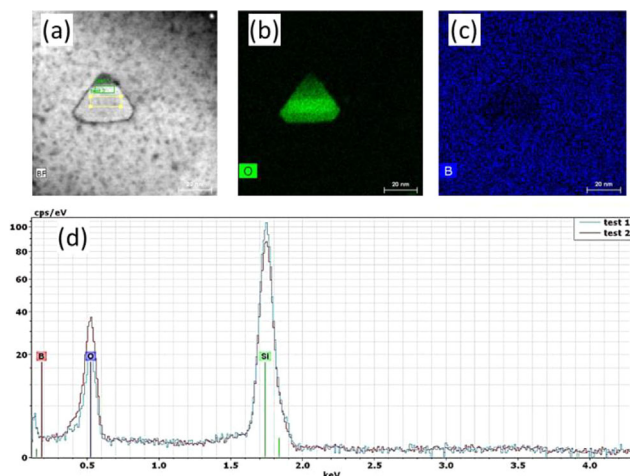
Figure 8. Bright Field image (a), EDX maps of O (b) and B (c) and EDX spectra measured at two different locations in oxygen precipitate.

The investigation results above show a very fast formation of stacking faults and a significantly low B concentration in the precipitates. These results agree with the nucleation model of Sueoka[9] based on a lower formation energy of the silicon self-interstitial in p^+ materials promoting the enhanced nucleation. The results do not contradict to Wijaranakula's model of the B_iO_i mobile species dissolving in the vicinity of oxygen precipitates. However, the results in this work do not support models where B is supposed to be incorporated in the precipitate with relatively high volume fraction.

4. Conclusions

In this work, we exploit different techniques to investigate oxygen precipitates and their growth in highly B-doped CZ Si wafers. In the wafers annealed at 1000 °C for various time following a stabilization anneal at 780 °C for 3 h octahedral precipitates were formed. Besides precipitates, dislocation loops and stacking faults were found. The dislocation loops disappear after longer annealing in contrast to the stacking faults which were detected in all the samples annealed at 1000 °C. The octahedral precipitates reach the very high density of 1×10^{13} cm^{-3} after short annealing. With increasing annealing time at 1000 °C, the precipitates split in two fractions, small and large precipitates. This process observed after 16 h proceeds very slowly in time. Such behavior could be explained by Ostwald ripening. The octahedral precipitates are composed of SiO_2 and the B concentration is below the detection limit of the EDX method used. This results support Sueoka's theory explaining enhanced precipitation in p^+ wafers by the lower formation energy of the silicon self-interstitials. They do not exclude Wijaranakula model of the B_iO_i mobile species dissolving in the vicinity of oxygen precipitates. We have also shown, that the OPE:C etchant can be a good alternative for determination of BMDs.

[1] M. Yonemura, K. Sueoka, K. Kamei, *J. Appl. Phys.* **2000**, *88*, 503.
[2] K. Sueoka, M. Akatsuka, M. Jonemura, T. Ono, E. Asayam, H. Katahama, *J. Electrochem. Soc.* **2000**, *147*, 756.
[3] W. Sugimura, T. Ono, S. Umeno, M. Hourai, K. Sueoka, *J. ESC Transactions* **2006**, *2*, 95.
[4] H. Takeno, K. Aihara, Y. Hayamizu, Y. Kitagawara, *Electrochem. Soc. Proc.* **1998**, *98-1*, 1012.
[5] H. Hieslmair, S. A. McHugo, A. A. Istratov, E. R. Weber, in *Properties of Crystalline Silicon* (Ed: R. Hull), INSPEC, London **1999**, Ch. 15.2.
[6] F. Secco d'Aragona, *J. Electrochem. Soc.* **1972**, *119*, 948.
[7] D. Kot, G. Kissinger, M. A. Schubert, A. Sattler, *ECS J. Solid State Sci. Technol.* **2014**, *3*, P370.
[8] D. Kot, G. Kissinger, M. A. Schubert, A. Sattler, *ECS J. Solid State Sci. Technol.* **2017**, *6*, N17.
[9] K. Sueoka, *ECS Transactions* **2006**, *3*, 71.
[10] W. Wijaranakula, *J. Appl. Phys.* **1992**, *72*, 2713.
[11] O. De Gryse, P. Clauws, J. Vanhellemont, O. I. Lebedev, J. Van Landuyt, E. Simoen, C. Claeys, *J. Electrochem. Soc.* **2004**, *151*, G598.
[12] O. De Gryse, J. Vanhellemont, P. Clauws, O. I. Lebedev, J. Van Landuyt, E. Simoen, C. Claeys, *Physica B* **2003**, *340–342*, 1013.
[13] W. Ostwald, *Z. Phys. Chem.* **1900**, *34*, 495.
[14] J. Will, A. Gröschel, C. Bergmann, E. Spiecker, A. Magerl, *J. Appl. Phys.* **2014**, *115*, 123505.
[15] K. Nakashima, T. Yoshida, Y. Mitsushima, *J. Electrochem. Soc.* **2005**, *152*, G339.
[16] T. Malis, S. C. Cheng, R. F. Egerton, *J. Electron Microscopy Technique* **1988**, *8*, 193.
[17] Y. Saito, Y. Matsushita, European Patent EP 0281115B1, 20 Sept **1994**.
[18] J. Mähliß, A. Abbadie, B. O. Kolbesen, *Mater. Sci. Eng. B* **2009**, *159–160*, 309.
[19] M. Pellowska, D. Possner, D. Kot, G. Kissinger, B. O. Kolbesen, *Sol. St. Phenom.* **2010**, *156–158*, 443.
[20] K. Sueoka, N. Ikeda, T. Yamamoto, S. Kobayashi, *J. Appl. Phys.* **1993**, *74*, 5437.
[21] J. Vanhellemont, *J. Appl. Phys.* **1995**, *78*, 4297.
[22] J. C. Mikkelsen, Jr., in *Oxygen, Carbon, Hydrogen, and Nitrogen in Silicon* (Eds: I. C. Mikkelsen, Jr., S. J. Pearton, J. W. Corbett, S. J. Pennycook), Materials Research Society, Princeton, NJ **1986**, p. 19.
[23] D. Kot, G. Kissinger, M. A. Schubert, M. Klingsporn, A. Huber, A. Sattler, *Phys. Status Solidi RRL* **2015**, *9*, 405.
[24] G. Kissinger, M. A. Schubert, D. Kot, T. Grabolla, *ECS J. Solid State Sci. Technol.* **2017**, *6*, N54.